

Quantum-enhanced microscopy with binary-outcome photon counting

G. R. Jin,^{1,*} W. Yang,^{2,†} and C. P. Sun^{2,‡}

¹Department of Physics, Beijing Jiaotong University, Beijing 100044, China

²Beijing Computational Science Research Center, Beijing 100084, China

(Dated: November 18, 2018)

A polarized light microscopy using path-entangled N -photon states (i.e., the N00N states) has been recently demonstrated to surpass the shot-noise limit at low flux illumination level. However, the microscopy images suffers from divergence of phase sensitivity, which inevitably reduces the quality of images. Here, we show that due to experimental imperfections, such a singularity is a common problem in quantum-enhanced microscopy that uses a finite N nonclassical state for illumination (e.g., the N00N states and the twin-Fock states). We propose two schemes to remedy this singularity: (i) locking the phase shift sensed by the beams at the optimal working point, using a spatially dependent offset phase, which can be fulfilled by a feedback loop in the microscopy; (ii) a combination of two binary-outcome coincidence detections with and without a fixed offset phase also works to completely eliminate the singularity. Our observations, valid for any kind of binary-outcome quantum measurement, open the way for realistic implementations of quantum imaging and quantum metrology with high N nonclassical states of light.

PACS numbers: 42.50.Dv, 06.30.Bp, 42.50.St

Light microscopy with low photon flux illumination is desirable to avoid damaging on the specimen (e.g., the biological samples) [1–5]. At the low light level, it might be more efficient to use nonclassical light for illumination, such as twin beams from a parametric down-conversion light [1] and amplitude squeezed light [2]. Recently, a polarized light microscopy using path-entangled N -photon states (i.e., the N00N states) $\sim (|N, 0\rangle + |0, N\rangle)$ is demonstrated to enlarge the contribution of each photon to the image contrast [4, 5], where $|m, n\rangle \equiv |m\rangle_H \otimes |n\rangle_V$ denotes a product of Fock states of two orthogonal polarization modes H and V . Performing a binary-outcome photon counting [4, 5], it is found that the birefringence phase shift of a sample $\phi(x, y)$ can be estimated beyond the shot-noise limit, i.e., the phase sensitivity $\delta\phi(x, y) < 1/\sqrt{N}$. However, the phase sensitivity diverges at certain values of phase shift, which in turn reduces the quality of microscopy images [5].

Compared with the N00N states, the twin-Fock states $|n, n\rangle$ are easier to prepare and more robust against photon loss [6–8]. Recently, it has been shown that the visibility of 6-photon counts rate can reach $\sim 94\%$ [8], significantly better than that of a five-photon N00N state [9]. In addition, the achievable phase sensitivity can surpass that of the N00N states with a binary-outcome photon counting [8]. Similar to Ref. [5], however, we will show that quantum-enhanced microscopy illuminated by the twin-Fock state of light (or any finite N input state) is also subject to the divergence of the phase sensitivity. In this Letter, we propose a scheme to avoid the singularity by locking the phase shift sensed by the beams at the optimal working point using a feedback offset phase at each pixel, as illustrated schematically by Fig. 1(a). We further show that a combination of two binary-outcome photon counting with and without a fixed offset phase also works to remove the singularity. Our results can be generalized to any kind of binary-outcome measurement that has been widely adopted in quantum metrology [10–16], and recently in quantum-enhanced

microscopy [4, 5].

Microscopy images reconstructed by inverting the signal.— To illustrate the role of the singularity on the image quality, we consider a quantum-enhanced microscopy illuminated by the twin-Fock states of light $|n, n\rangle$ [6–8], with the number of photons $N = 2n$. For a transparent sample (see Fig. 1(a)), the microscopy images can be constructed from coincidence photon counts at the output ports [4, 5]. The probability for detecting exactly n_1 photons in the H polarization mode and n_2 photons in the V polarization mode is given by

$$P(n_1, n_2|\theta) = |\langle n_1, n_2 | e^{-i[\varphi + \phi(x, y)]J_y} | n, n \rangle|^2, \quad (1)$$

where φ is a controlled offset phase, $\phi(x, y)$ denotes spatially dependent phase shift caused by birefringence of the polarized beams that passing through a sample [5], and $\theta(x, y) = \varphi + \phi(x, y)$. The phase accumulation $\exp(-i\theta J_y)$ can be realized with a Mach-Zehnder interferometer [17–19], corresponding to a rotation around the y -component of the Stokes vector $\mathbf{J} = (a_H^\dagger, a_V^\dagger)\sigma(a_H, a_V)^T/2$, where a_H (a_V) is the annihilation operator of the polarization mode H (V), and σ denotes the Pauli operator.

The photon counting with the specific event $n_1 = n_2 = n$ is of interest [7, 8], which can be treated as a projection measurement (i.e., the single-fringe detection [8]), with the output signal $\langle \mu(\theta) \rangle \equiv \text{Tr}[\mu\rho(\theta)] = P(n, n|\theta)$, where $\mu = |n, n\rangle\langle n, n|$ is a projection operator and $\rho(\theta) = \exp(-i\theta J_y)\rho_{\text{in}}\exp(i\theta J_y)$ denotes the output state. For each a given phase shift θ , performing the photon counting for N times, the signal is measured by the normalized counts rate $P(n, n|\theta) \simeq N_{n,n}/N$, where $N_{n,n}$ denotes the occurrence number of the event $n_1 = n_2 = n$. In Fig. 1(c), we numerically simulate experimental results of Refs. [7, 8], using N random numbers $\{\xi_1, \xi_2, \dots, \xi_N\}$, with $\xi_k \in [0, 1]$. The occurrence number $N_{n,n}$ can be obtained by counting how many values of $\xi_k \in [0, P(n, n|\theta)]$, where, to take experimental imperfections into account, we make a replacement $P(n, n|\theta) \rightarrow a_0 P(n, n|\theta) + b_0$, with a_0 and b_0 related

to imperfect visibility and reduced peak height at the phase origin [20]. Statistical average of $N_{n,n}/N$ and its standard deviation can be obtained after 20 replicas of the measurements, as depicted by the circles and the bars of Fig. 1(c). Finally, we fit the circles to obtain $P_{\text{fit}}(n, n|\theta)$ (see the blue solid lines), as done in Refs. [7, 8]. One can see that the probabilities show multi-fold oscillations and the first dark fringe appears at $\theta_{\text{dark}} \simeq \pi/2$, $\arccos(\sqrt{1/3})$, and $\arctan(\sqrt{2/3})$, from top to bottom, as depicted in Fig. 1(c).

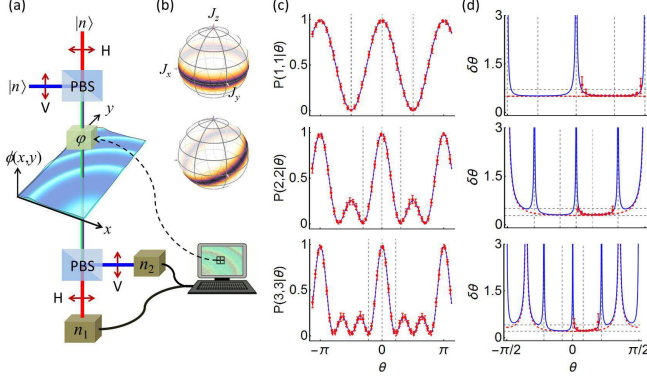


FIG. 1: Schematic plot of polarized light microscopy with feed-back control (a), and quasi-probability distribution of the input twin-Fock states $|n, n\rangle$ on Poincare sphere (b) and that of the output state $\exp(-i\theta J_y)|n, n\rangle$, with $\theta = \varphi + \phi(x, y)$. Photon counting over the output state, the conditional probability $P(n_1, n_2|\theta)$ is measured by normalized coincidence rate for the event $n_1 = n_2 = n$ (c), which in turn gives phase sensitivity (d). The colinear Mach-Zehnder interferometer in (a) includes polarizing beam splitter (PBS), phase accumulation, and another PBS. The circles and the bars: statistical averages of $N_{n,n}/N$ (c) and $\sqrt{N}\sigma$ (d), for number of photon counts $N = 100$, and their standard deviations after 20 replicas of the measurements, where σ is given by Eq. (7); see text. Red dashed (blue solid) lines in (c) and (d): exact (fitting) results of $P(n, n|\theta)$, and the associated sensitivities $\delta\theta$. Vertical lines in (c) and (d) indicate locations of the phase origin, the first dark fringe at $\pm\theta_{\text{dark}}$, and the optimal working point for phase sensing at $\pm\theta_{\text{min}}$. The horizontal lines in (d): the shot-noise limit $1/\sqrt{N}$ and the quantum Cramer-Rao bound $\sqrt{2}/\sqrt{N(N+2)}$ for $N = 2n = 2, 4, 6$.

The phase estimator obtained by inverting the averaged signal (i.e., the inversion estimator θ_{est}) has been used to reconstruct the microscopy images [5]. The image quality is therefore determined by phase uncertainty of θ_{est} , which is indeed a solution of $P(n, n|\theta) = N_{n,n}/N$ within a monotonic regime, e.g., $\theta \in (0, \theta_{\text{dark}})$. According to linear error propagation, the phase uncertainty is quantified by $\delta\theta = \Delta\mu/|\partial\langle\mu(\theta)\rangle/\partial\theta|$, where, for a single-shot measurement, the fluctuations of signal $(\Delta\mu)^2 \equiv \langle\mu^2\rangle - \langle\mu\rangle^2 = P(n, n|\theta)[1 - P(n, n|\theta)]$, as $\mu^2 = \mu$. In Fig. 1(d), we plot the phase sensitivity as a function of θ , using exact (fitted) results of $P(n, n|\theta)$. For the exact cases (the red dashed lines), the sensitivity reaches minimum at the phase origin [7]. Due to experimental imperfections, the sensitivity diverges at certain values of θ (e.g., $\theta = 0, \pm\theta_{\text{dark}}$). This is because the slope of signal $\partial\langle\mu(\theta)\rangle/\partial\theta = 0$ at that

points, but $\Delta\mu \neq 0$ (see also Ref. [20]), leading to $\delta\theta \rightarrow \infty$. Such a singularity could take place for any finite N input state, e.g., a single-photon state $|1, 0\rangle$ and the multi-photon N00N states [5]. From the blue solid lines of Fig. 1(d), one can see the optimal working point for phase sensing $\theta_{\text{min}} \simeq 0.88, 0.37$, and 0.26 ($\sim 15^\circ$ [8]), with the best sensitivity beating the shot-noise limit by a factor $\eta = 1/(\sqrt{N}\delta\theta_{\text{min}}) \simeq 1.39$ (for $N = 2$), 1.61 ($N = 4$), and 1.85 ($N = 6$).

Figure 2 shows the microscopy images reconstructed from the inversion estimator for the input twin-Fock states $|n, n\rangle$ with $n = N/2 = 1, 2, 3$, and that of the single-photon state $|1, 0\rangle$. The birefringence phase shift used here is $\phi(x, y) = 0.1 + 0.437 \cos^6[2(x - \pi/2)^2 + y^2] \in (0.1, 0.537]$; see Fig. 1(a) and Fig. 3(d). Following Ref. [5], the offset phase φ is tuned such that the total phase shift sensed by the beams $\theta = \varphi + \phi(x, y) \in [\theta_{\text{min}}, \theta_{\text{dark}}]$ [21], where θ_{dark} denotes the location of the first dark fringe, and θ_{min} the optimal working point for phase sensing, as shown in Fig. 1(c) and (d). Performing the photon counting measurement and inverting the signal, one can obtain the estimator $\phi_{\text{est}}(x, y) = \theta_{\text{est}}(x, y) - \varphi$ at each spatial point, where θ_{est} a solution of $P_{\text{fit}}(n, n|\theta) = N_{n,n}/N$ within the monotonic regime, as mentioned above. To keep a finite number of photons at each pixel, we use a fixed resource $N \times N = 600$. As shown in Fig. 2(d), one can note that the estimator $\phi_{\text{est}}(x, y)$ is *less* accurate at some spatial points (see the speckles). This is because the total phase shift sensed by the beams $\theta = \varphi + \phi(x, y) \sim \theta_{\text{dark}}$, at which the phase sensitivity diverges. Similar phenomenon also takes place for the triphoton N00N state [5], and any finite N input state.

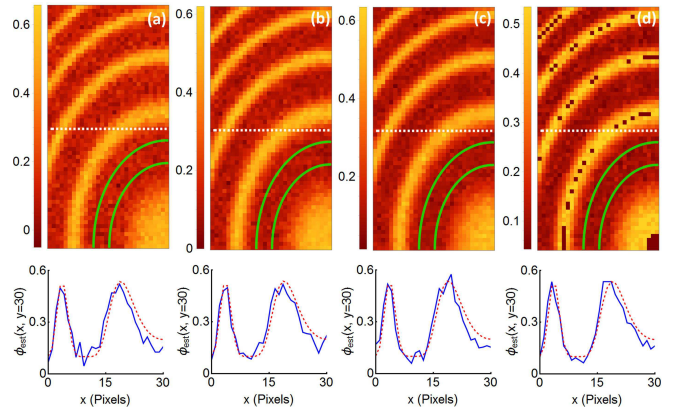


FIG. 2: Microscopy images of 30×60 pixels reconstructed from the phase estimator $\phi_{\text{est}}(x, y)$ for a single-photon state (a), and twin-Fock states with $N = 2n = 2$ (b), 4 (c), and 6 (d). The estimator at each pixel is given by $\phi_{\text{est}} = \theta_{\text{est}} - \varphi$, where θ_{est} is obtained by performing the coincidence detection and then inverting the signal, and the offset phase φ is tuned such that $\theta = \varphi + \phi(x, y) \in [\theta_{\text{min}}, \theta_{\text{dark}}]$. Within the area enclosed by the green solid lines, the phase shift sensed by the beams is almost optimal, i.e., $\theta \approx \theta_{\text{min}}$. The bottom panels: the estimator at the pixel $y = 30$ as a function of x (blue solid), in comparison with the true value of phase shift of the sample (red dashed). The number of measurements: $N = 600$ (a), 300 (b), 150 (c), 100 (d), to keep exactly 600 photons at each pixel.

The image quality is improved with the quantum source of light as long as the sensed phase shift is far from the singular points. To quantify such an improvement, we calculate standard deviation of the estimators within a local area that enclosed by the green solid lines of Fig. 2. Hereafter, the local standard deviation is denoted as $\text{LSD}_{|\psi\rangle}$ for $|\psi\rangle$. Similar to Ref. [5], we focus on the relative noise $\text{LSD}_{|1,0\rangle}/\text{LSD}_{|n,n\rangle}$, which gives a measure of the improvement in the image quality beyond the classical illumination. From each image of Fig. 2, one can extract the value of $\text{LSD}_{|\psi\rangle}$ and hence the relative noise. Taking 20 pictures for each state, we obtain the averaged values $\text{LSD}_{|1,0\rangle} = 0.0413$, $\text{LSD}_{|1,1\rangle} = 0.0297$, $\text{LSD}_{|2,2\rangle} = 0.0253$, and $\text{LSD}_{|3,3\rangle} = 0.022$, which gives $\text{LSD}_{|1,0\rangle}/\text{LSD}_{|n,n\rangle} = 1.39$ (for $n = N/2 = 1$), 1.63 ($n = 2$), and 1.88 ($n = 3$), in agreement with the expected factor η .

Theoretically, the enhanced factor can be predicted by quantum Fisher information of a phase-encoded state $\exp(-i\theta G)|\psi_{\text{in}}\rangle$, where G is a hermitian operator that encodes a phase shift on the input state $|\psi_{\text{in}}\rangle$. For the pure-state case, the Fisher information is given by $F_Q = 4(\langle G^2 \rangle_{\text{in}} - \langle G \rangle_{\text{in}}^2)$, which sets a bound on the phase sensitivity, known as quantum Cramer-Rao bound [22–24]: $\delta\theta_{\text{QCRB}} = 1/\sqrt{F_Q}$. The choice of phase generator G is fully determined by quantum correlation of the input state [25–29]. For the twin-Fock states $|n, n\rangle$, the quasi-probability distribution spreads along the equator of Poincare sphere, as shown by Fig. 1(b), implying that the generator can take the form $G = J_x \cos \alpha + J_y \sin \alpha$ for arbitrary α ($= \pi/2$ in Eq. (1)), for which $F_Q = N(N+2)/2 \sim O(N^2)$. As a result, the improvement in the sensitivity attainable from the twin-Fock states is $\eta = 1/(\sqrt{N}\delta\theta_{\text{QCRB}}) = \sqrt{(N+2)/2}$.

Phase locking to avoid the singularity.—Due to the divergence of the sensitivity, the sensing range of a quantum-enhance microscopy becomes narrow, especially when a higher N nonclassical state is injected. In order to remedy this problem, we propose a scheme to control the offset phase at each spatial point according to three estimators nearby, as illustrated schematically by Fig. 1(a).

The basic idea of our scheme is to lock the sensed phase shift at the optimal working point, i.e., $\theta = \varphi(x, y) + \phi(x, y) \sim \theta_{\text{min}}$, using a spatial dependent offset phase $\varphi(x, y)$. Thus, we can avoid the divergence of the phase sensitivity. To achieve this goal, we first estimate the true value of phase shift at a single pixel, e.g., $\phi(0, 0) = \phi_{\text{est}}(0, 0) \approx 0.1\text{rad}$. From the starting point, we scan the beams horizontally and vertically to obtain all the estimators $\phi_{\text{est}}(i, 0)$ and $\phi_{\text{est}}(0, j)$, using the offset phase determined by $\phi_{\text{est}}(i-1, 0)$ and $\phi_{\text{est}}(0, j-1)$. Next, we adjust the offset phase according to three estimators in a rectangle that contains four pixels, as illustrated in Figs. 3(a) and (b).

Specially, to estimate $\phi(1, 0)$, we adjust the offset phase as $\varphi(1, 0) = \theta_{\text{min}} - \phi_{\text{est}}(0, 0)$, which ensures $\varphi(1, 0) + \phi(1, 0) \approx \theta_{\text{min}}$, provided $\phi(1, 0) \approx \phi_{\text{est}}(0, 0)$. Performing the photon counting measurement and inverting the signal, we obtain a local phase estimator $\phi_{\text{est}}(1, 0) = \theta_{\text{est}} - \varphi(1, 0)$, where θ_{est} is a solution of $P_{\text{fit}}(n, n|\theta) = N_{n,n}/N$, as mentioned above. Similarly, one can obtain the estimator $\phi_{\text{est}}(0, 1)$. To estimate $\phi(1, 1)$, we use the three estimators in a rectangle (see

Fig. 3(a)) and adjust the offset phase as $\varphi(1, 1) = \theta_{\text{min}} - [\phi_{\text{est}}(0, 1) + \phi_{\text{est}}(0, 0) + \phi_{\text{est}}(1, 0)]/3$, which improves succeed probability for the phase locking $\varphi(1, 1) + \phi(1, 1) \approx \theta_{\text{min}}$. Repeating the above process, one can extract the phase information of a sample over all the pixels, as shown in Fig. 3(c).

In Fig. 3(c), we show the microscopy image for the six-photon state $|3, 3\rangle$ using the method of phase locking. The main advantage of this method is that the singular points (i.e., the speckles) disappear. It seems likely that the sensed phase shift at each pixel has been dragged back to the optimal working point. The overall quality of the image is improved in a comparison with that of Fig. 2(d). One can see this from the mean squared error (MSE) between the estimator and its true value of phase shift, i.e., $\text{MSE} = \sum_{i,j} [\phi_{\text{est}}(i, j) - \phi(i, j)]^2 / N_{\text{pixels}}$, where $\phi(i, j)$ is depicted in Fig. 3(d) and N_{pixels} denotes total number of pixels. Interestingly, it is found $\sqrt{\text{MSE}} \sim 0.022$, in agreement with the local noise $\text{LSD}_{|3,3\rangle}$. This observation implies that at most of pixels, the phase shift sensed by the beams is optimal. We confirm this by directly evaluating the root-mean-squared error for the input states $|1, 0\rangle$, $|1, 1\rangle$, and $|2, 2\rangle$. The phase locking scheme requires control of the offset phase at each spatial point, which, in general, can be fulfilled by a feedback loop.

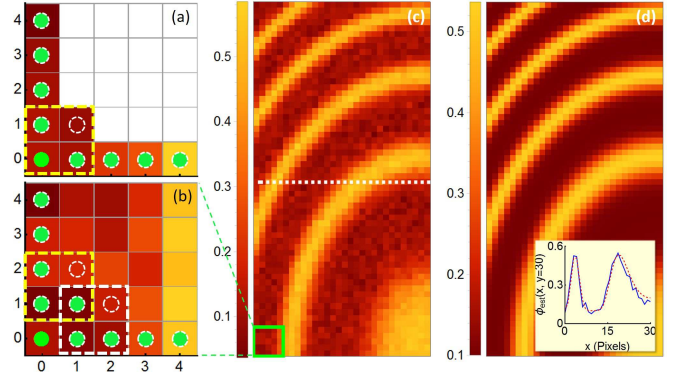


FIG. 3: Two steps of the phase locking (a) and (b), and the microscopy image of the six-photon twin-Fock state (c) in a comparison with the true value of phase shift (d). In (a), the offset phase is tuned as $\varphi(i, 0) = \theta_{\text{min}} - \phi_{\text{est}}(i-1, 0)$, and $\varphi(0, j) = \theta_{\text{min}} - \phi_{\text{est}}(0, j-1)$; in (b), it becomes $\varphi(i, j) = \theta_{\text{min}} - [\phi_{\text{est}}(i-1, j) + \phi_{\text{est}}(i, j-1) + \phi_{\text{est}}(i-1, j-1)]/3$, where θ_{min} is the optimal working point for phase sensing, and ϕ_{est} can be obtained by the coincidence detections and the inversion of the signal. The total number of photon counts in (c) is $N = 100$ to ensure 600 photons at each pixel. The inset in (d): a comparison of the estimator (blue solid) and the true value of phase shift (red dashed) at the pixel $y = 30$.

Maximum likelihood estimator for a binary-outcome measurement.—The above results can be generalized to any kind of binary-outcome measurement, for which the output signal is given by

$$\langle \mu(\theta) \rangle = \sum_{i=\pm} \mu_i P(i|\theta) \approx \sum_{i=\pm} \mu_i \frac{N_i}{N}, \quad (2)$$

where N_{\pm}/N denotes the occurrence frequency of the outcome μ_{\pm} , measured by the normalized coincidence rate with a finite number of photon counts $N = N_+ + N_-$. For the input twin-Fock states, the specific detection event $n_1 = n_2 = n$ can be treated as the outcome “+” and the others as “−”, with the conditional probability $P(+|\theta) \equiv P(n, n|\theta)$ and hence $P(-|\theta) = 1 - P(+|\theta)$. Taking $\mu_+ = +1$ and $\mu_- = 0$, the signal becomes $\langle \mu(\theta) \rangle = P(+|\theta) = P(n, n|\theta)$, as expected. Similarly, the parity detection gives two outcome ± 1 , according to even or odd number of photons being detected at one port of the interferometer [10–13]. Recently, quantum-enhanced microscopy with a two-photon N00N state has been demonstrated by counting odd number of photons [4]. For a measurement with continuous-variable outcome, one can also realize a binary-outcome measurement by dividing the data into two bins [15]. These cases are indeed binary-outcome measurement [16].

For any kind of binary-outcome measurement, the inversion estimator θ_{est} can be obtained by inverting the averaged signal, which is indeed a solution of Eq. (2), or equivalently $P(+|\theta) = N_+/N$, independently from the values μ_{\pm} . According to the error propagation, the uncertainty of θ_{est} depends on the fluctuations of signal $\Delta\mu = (\mu_+ - \mu_-)\Delta N_+/N$, with $\Delta N_+ = \sqrt{NP(+|\theta)P(-|\theta)}$ being standard deviation of a binomial distribution:

$$\mathcal{L}(\theta; N_+) = \binom{N}{N_+} [P(+|\theta)]^{N_+} [P(-|\theta)]^{N_-}, \quad (3)$$

where $\binom{n}{k}$ is the binomial coefficient, and $\sum_{N_+} \mathcal{L}(\theta; N_+) = [P(+|\theta) + P(-|\theta)]^N = 1$. On the other hand, from Eq. (2), we obtain the slope of signal $\partial\mu(\theta)/\partial\theta = (\mu_+ - \mu_-)\partial P(+|\theta)/\partial\theta$, which, together with $\Delta\mu$, gives the phase uncertainty

$$\delta\theta = \frac{\Delta\mu}{|\partial\mu(\theta)/\partial\theta|} = \frac{\sqrt{P(+|\theta)P(-|\theta)}}{\sqrt{N}|\partial P(+|\theta)/\partial\theta|} = \frac{1}{\sqrt{NF(\theta)}}, \quad (4)$$

where, for a single-shot measurement, the classical Fisher information is given by

$$F(\theta) = \sum_{i=\pm} \frac{1}{P(i|\theta)} \left[\frac{\partial P(i|\theta)}{\partial\theta} \right]^2. \quad (5)$$

As our main result, Eq. (4) indicates that for any kind of binary-outcome measurement [10–16], the phase uncertainty of θ_{est} always saturate the Cramer-Rao lower bound $\sim 1/\sqrt{F(\theta)}$. This is somewhat counter intuitive since, according to Fisher’s theorem [30], this bound is saturable by the maximum likelihood estimator (MLE) as the number of measurements $N \gg 1$. To understand it, we further investigate the MLE by finding a value of θ that maximizes Eq. (3); Hereinafter, denoted by θ_{mle} . When $N_{\pm} \sim O(N) \gg 1$, the binomial distribution of $\mathcal{L}(\theta; N_+)$ becomes normal

$$\mathcal{L}(\theta; N_+) \propto \exp\left(-\frac{[N_+ - NP(+|\theta)]^2}{2(\Delta N_+)^2}\right), \quad (6)$$

which indicates that the MLE θ_{mle} also satisfy the equation $P(+|\theta) = N_+/N$, the same with that of θ_{est} . This result keeps hold for any input state of the probes and is independent from any specific form of the noise.

For the input twin-Fock states, we calculate the phase uncertainty of θ_{mle} using $P_{\text{fit}}(n, n|\theta)$; see the blue solid lines of Fig. 1(d). To avoid the phase ambiguity [31–33], we introduce prior knowledge about the true value of θ by assuming the prior probability $P(\theta) = 1$ for $\theta \in [0, \theta_{\text{dark}}]$ and 0 outside. Next, we fit the phase distribution as a Gaussian around its peak [34], i.e., $\mathcal{P}(\theta|N_+) = C\mathcal{P}(\theta)\mathcal{L}(\theta; N_+) \simeq C \exp[-(\theta - \theta_{\text{mle}})^2/(2\sigma^2)]$, where C is a normalized factor and σ is 68.3% confidence interval of the Gaussian, given by

$$\sigma \simeq \sqrt{\frac{C}{|\partial^2 \mathcal{P}(\theta|N_+)/\partial\theta^2|_{\theta_{\text{mle}}}}}. \quad (7)$$

Statistical average of $\sqrt{N}\sigma$ and its standard deviation, as depicted by the circles and the bars of Fig. 1(d), show a good agreement with the blue solid lines.

So far, we have shown that for any kind of binary-outcome measurement, the inversion estimator θ_{est} is indeed the same with the MLE θ_{mle} . For a finite N twin-Fock states, both of them suffer from the singularity of the phase sensitivity (e.g., see Fig. 1(d)), which reduces the image quality. This problem can not be completely avoided even when all the contributions of $(N+1)$ outcomes are taken into account.

A combination of two photon counting measurements.— Finally, it should be mentioned that the phase locking scheme in Fig. 3 requires a feedback loop, which may be quite costly in terms of experimental time and resource. In order to reduce experimental cost, one can use a fixed offset phase φ , as done in Ref. [5], but instead separates the total measurements into two parts: the binary-outcome photon counting with and without the offset phase.

In the absence of the control phase, performing the coincidence detection over the output state $\exp(-i\phi J_y)|n, n\rangle$ for N_1 times, one can obtain the probability for detecting the outcome “+” as $P(+|\phi) \simeq N_1^{(+)} / N_1$, where the occurrence frequency $N_1^{(+)} / N_1$ is measured by the normalized coincidence rate of the event $n_1 = n_2 = n$ (i.e., the outcome “+”). Applying a fixed offset phase in the path, and then performing the measurements for N_2 times gives the conditional probability $P(+|\phi') \simeq N_2^{(+)} / N_2$, with $\phi' = \phi + \varphi$. In the upper panel of Fig. 4, we plot statistical average of the coincidence rates (the circles) after 20 replicas of the measurements, and fit them as the blue solid (red dashed) lines. These two probabilities oscillate with ϕ and therefore can be used to estimate the birefringence phase shift of a sample.

As a combination of two binary-outcome measurements with the total number of photon counts $N_1 + N_2 = N \gg 1$, it is straightforward to retrieve the estimator ϕ_{mle} by maximizing the likelihood function:

$$\mathcal{L}(\phi) \propto [P(+|\phi)]^{N_1^{(+)}} [1 - P(+|\phi)]^{N_1 - N_1^{(+)}} \times [P(+|\phi')]^{N_2^{(+)}} [1 - P(+|\phi')]^{N_2 - N_2^{(+)}} \quad (8)$$

where $\phi' = \phi + \varphi$, as mentioned above, and $N_k^{(+)} / N_k$ denotes the occurrence frequency of the outcome “+” in the k th measurement (with $k = 1, 2$). Using the fitting results of $P(+|\phi)$ and $P(+|(\phi + \varphi))$, we obtain the MLE ϕ_{mle} and its uncertainty by numerically calculating the peak of the likelihood function and the 68.3% confidence interval around the peak (i.e., the MLE). From the inset of Figs. 4(d)-(f), one can see the statistical average of the MLE $\langle \phi_{\text{mle}} \rangle_s = \phi$, indicating that the MLE is unbiased. In addition, the averaged value of $\sqrt{N}\sigma$ does not show any singularity (see the circles). It follows the effective phase sensitivity $\delta\phi \equiv \sqrt{N} / \sqrt{F_{\text{tot}}(\phi)}$, as shown by the blue solid lines of Figs. 4(d)-(f), where $F_{\text{tot}}(\phi) = N_1 F(\phi) + N_2 F(\phi + \varphi)$ denotes the total Fisher information and $F(\phi)$ is given by Eq. (5).

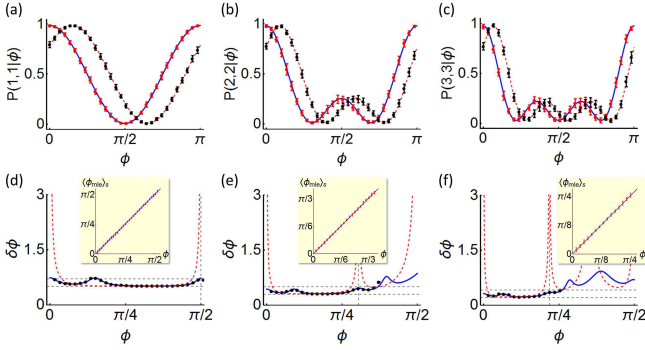


FIG. 4: Normalized coincidence rates (a)-(c) and effective phase sensitivities (d)-(f), using the input twin-Fock states $|1, 1\rangle$ (left), $|2, 2\rangle$ (middle), and $|3, 3\rangle$ (right). The offset phase is chosen as $\varphi = -0.3 \times \theta_{\text{dark}}$ with the location of θ_{dark} indicated by the vertical dashed lines in (d)-(f). The number of measurements: $N_1 = N_2 = N/2$, with $N \times N = 1200$ fixed. The circles and the bars: statistical average of $N_{n,n}/N$ and $\sqrt{N}\sigma$, as well as their standard deviation after 20 replicas of the measurements (with σ given by Eq.(7)). Solid lines: fitting curves of the averaged counts rate, and the associated phase sensitivities with (without) the control phase (red dashed lines). The inset in (d)-(f) indicates that the MLE is unbiased, due to $\langle \phi_{\text{mle}} \rangle_s = \phi$. The horizontal lines: the shot-noise limit $1/\sqrt{N}$ and the quantum Cramer-Rao bound $\sqrt{2}/\sqrt{N(N+2)}$.

Obviously, the singularity of $\delta\phi$ can be completely eliminated by a suitable choice of the offset phase φ . This is in sharp contrast to the previous results [5, 21]. One can also see this from Fig. 1(d), where the sensitivity diverges at θ_{dark} , with its location indicated by the vertical dashed lines of Figs. 4(d)-(f). Using the control phase, however, the achievable sensitivity can surpass the shot-noise limit as ϕ increases up to $\sim 1.2 \times \theta_{\text{dark}}$. It is therefore useful to sense the birefringence phase shift of a sample $|\phi(x, y)| > \theta_{\text{dark}}$ at the sub-shot noise limit.

Conclusion.—Quantum-enhanced microscopy with the input twin-Fock states has been investigated to eliminate the singularity of the phase sensitivity. Using spatially dependent offset phase, we found that the phase shift sensed by the beams can be locked at the optimal working point. The overall image quality is found better than classical light illu-

mination by a factor $\sim \sqrt{(N+2)/2}$. We further show that a combination of two binary-outcome photon counting with and without a fixed offset phase also works to remove the singularity. The proposed schemes can be immediately used in the triphoton experiment [5] to improve the overall quality. Our results keep valid for any kind of binary-outcome measurement and pave the way for realistic implementations of quantum imaging and quantum metrology that uses high N nonclassical states of light.

We would like to thank S. Rosen and Y. Silberberg for kindly response to our questions, as well as P. Liu and T. Li for their assistance in plotting the figures. This work has been supported by the National Natural Science Foundation of China (Grant Nos. 11421063, 11534002, 11274036, and 11322542), the National 973 program (Grant Nos. 2012CB922104, 2014CB921403, and 2014CB848700).

* Electronic address: grjin@bjtu.edu.cn

† Electronic address: wenyang@csrc.ac.cn

‡ Electronic address: cpsun@csrc.ac.cn

- [1] G. Brida, M. Genovese, and I. R. Berchera, *Nat. Photonics* **4**, 227 (2010).
- [2] M. A. Taylor, J. Janousek, V. Daria, J. Knittel, B. Hage, H.-A. Bachor, and W. P. Bowen, *Nat. Photonics* **7**, 229 (2013).
- [3] G. B. Lemos, V. Borish, G. D. Cole, S. Ramelow, R. Lapkiewicz, and A. Zeilinger, *Nature (London)* **512**, 409 (2014).
- [4] T. Ono, R. Okamoto, and S. Takeuchi, *Nat. Commun.* **4**, 3426 (2013).
- [5] Y. Israel, S. Rosen, and Y. Silberberg, *Phys. Rev. Lett.* **112**, 103604 (2014).
- [6] M. J. Holland and K. Burnett, *Phys. Rev. Lett.* **71**, 1355 (1993).
- [7] F. W. Sun, B. H. Liu, Y. X. Gong, Y. F. Huang, Z. Y. Ou, and G. C. Guo, *Europhys. Lett.* **82**, 24001 (2008).
- [8] G. Y. Xiang, H. F. Hofmann, and G. J. Pryde, *Sci. Rep.* **3**, 2684 (2013).
- [9] I. Afek, O. Ambar, and Y. Silberberg, *Science* **328**, 879 (2010).
- [10] J. J. Bollinger, W. M. Itano, D. J. Wineland, and D. J. Heinzen, *Phys. Rev. A* **54**, R4649 (1996).
- [11] J. P. Dowling, *Contemp. Phys.* **49**, 2 (2008); Y. Gao, C. F. Wildfeuer, P. M. Anisimov, H. Lee, and J. P. Dowling, *J. Opt. Soc. Am. B* **27**, A170 (2010).
- [12] C. C. Gerry and J. Mimih, *Contemp. Phys.* **51**, 497 (2010).
- [13] L. Cohen, D. Istrati, L. Dovrat, and H. S. Eisenberg, *Opt. Express* **22**, 11945 (2014).
- [14] D. Brivio, S. Cialdi, S. Vezzoli, B. Teklu, M. G. Genoni, S. Olivares, and M. G. A. Paris, *Phys. Rev. A* **81**, 012305 (2010).
- [15] E. Distant, M. Jezek, and U. L. Andersen, *Phys. Rev. Lett.* **111**, 033603 (2013).
- [16] X. M. Feng, G. R. Jin, and W. Yang, *Phys. Rev. A* **90**, 013807 (2014).
- [17] B. Yurke, S. L. MacCall, and J. R. Klauder, *Phys. Rev. A* **33**, 4033 (1986).
- [18] B. C. Sanders and G. J. Milburn, *Phys. Rev. Lett.* **75**, 2944 (1995).
- [19] T. Kim, O. Pfister, M. J. Holland, J. Noh, and J. L. Hall, *Phys. Rev. A* **57**, 4004 (1998).
- [20] See Supplemental Material for the detailed numerical simulations.

- [21] Using the method of Ref.[5], the sensing range of a quantum-enhanced microscopy is about $|\theta_{\text{dark}} - \theta_{\text{min}}|$, limited by the optimal work point for phase sensing θ_{min} and the location of dark fringe θ_{dark} nearby.
- [22] C. W. Helstrom, Quantum Detection and Estimation Theory (Academic, New York, 1976).
- [23] S. L. Braunstein and C. M. Caves, Phys. Rev. Lett. **72**, 3439 (1994); S. L. Braunstein, C. M. Caves, and G. J. Milburn, Ann. Phys. (N.Y.) **247**, 135 (1996).
- [24] V. Giovannetti, S. Lloyd, and L. Maccone, Nat. Photonics **5**, 222 (2011).
- [25] M. Kitagawa and M. Ueda, Phys. Rev. A **47**, 5138 (1993).
- [26] D. J. Wineland, J. J. Bollinger, M. W. Itano, and D. J. Heinzen, Phys. Rev. A **50**, 67 (1994); D. Leibfried *et al.*, Science **304**, 1476 (2004).
- [27] J. Ma, X. Wang, C. P. Sun, and F. Nori, Phys. Rep. **509**, 89 (2011).
- [28] L. Pezze and A. Smerzi, Phys. Rev. Lett. **102**, 100401 (2009); G. Toth, Phys. Rev. A **85**, 022322 (2012).
- [29] B. Lucke *et al.*, Science **334**, 773 (2011).
- [30] R. A. Fisher, Theory of statistical estimation, Proc. Cambridge Philos. Soc. **22**, 700 (1925).
- [31] L. Pezze and A. Smerzi, Europhys. Lett. **78**, 30004 (2007).
- [32] B. L. Higgins, D. W. Berry, S. D. Bartlett, H. M. Wiseman, and G. J. Pryde, Nature (London) **450**, 393 (2007).
- [33] D. W. Berry, B. L. Higgins, S. D. Bartlett, M. W. Mitchell, G. J. Pryde, and H. M. Wiseman, Phys. Rev. A **80**, 052114 (2009).
- [34] L. Pezze, A. Smerzi, G. Khoury, J. F. Hodelin, and D. Bouwmeester, Phys. Rev. Lett. **99**, 223602 (2007); L. Pezze and A. Smerzi, *ibid.* **100**, 073601 (2008).
-

SUPPLEMENTARY MATERIAL

In the following we present the details in numerical simulations.

Following Ref. [1], we consider a single-photon state $|1, 0\rangle$ as the input state to simulate the microscopy with a classical illumination. From Eq. (1) in the main text, we obtain the probability for detecting a single photon in the horizontal polarization mode and zero photon in the vertical polarization mode $P(1, 0|\theta) = |\langle 1, 0 | \exp(-i\theta J_y) | 1, 0 \rangle|^2 = \cos^2(\theta/2)$, conditioned on an unknown phase shift θ . If we treat the detection event $n_1 = 1$ and $n_2 = 0$ as the outcome “+”, and the others as “−”, then this is indeed a binary-outcome photon counting measurement, with the output signal $\langle \mu(\theta) \rangle = P(1, 0|\theta)$.

Performing the photon counting for N times, from Eq. (4), one can immediately obtain the phase sensitivity $\delta\theta = \Delta\mu/|\partial\langle\mu(\theta)\rangle/\partial\theta| = 1/\sqrt{NF(\theta)}$, where, for the single-photon input state, the classical Fisher information is given by

$$F(\theta) = \frac{[\partial P(1, 0|\theta)/\partial\theta]^2}{P(1, 0|\theta)[1 - P(1, 0|\theta)]} = 1. \quad (9)$$

In real experiment, e.g., Ref. [1], the achievable sensitivity depends on the true value of phase shift, arising from the detection efficiency, the photon loss, the imperfect visibility, and so on. To take the experimental imperfections into account, we first rewrite the conditional probability as

$$P(n_1, n_2|\theta) \rightarrow \frac{2hV}{1+V}P(n_1, n_2|\theta) + \frac{h(1-V)}{1+V}, \quad (10)$$

where the peak height h and the visibility V , as shown in Table I, can be determined by a photon-counting measurement. Next, we randomly choose N values of the outcomes according to $P(n_1, n_2|\theta)$ with a given θ [2]. For a binary-outcome measurement, only a specific detection event $\{n_1, n_2\}$ is of interest, e.g., $n_1 = 1$ and $n_2 = 0$. Thus, we generate N random numbers $\{\xi_1, \xi_2, \dots, \xi_N\}$, where $\xi_k \in [0, 1]$ for $k = 1, 2, \dots, N$. If $0 \leq \xi_k < P(1, 0|\theta)$, we set $\xi_k = +1$, otherwise, $\xi_k = 0$, then the number of “+1” can be used to simulate the occurrence number of the event $n_1 = 1$ and $n_2 = 0$, denoted as $N_{1,0}$. Finally, for each a given $\theta \in [-\pi, \pi]$, we repeat the above simulations for M times to obtain statistical average and standard deviation of the occurrence number. The averaged value of $N_{1,0}/N$ can be fitted as $P_{\text{fit}}(1, 0|\theta) = \langle N_{1,0}/N \rangle_s$, where $\langle (\dots) \rangle_s \equiv \sum_{i=1}^M (\dots)_i / M$ denotes the statistical average and M the number of simulations.

In Fig. 5, we numerically simulate the photon counting measurement for the single-photon input state $|1, 0\rangle$, using the parameters in Table I. With $N = 100$ and $M = 20$, we obtain $P_{\text{fit}}(1, 0|\theta) = aP(1, 0|\theta) + b$, with $a = 0.988$ and $b = 0.00396$. Substituting $P_{\text{fit}}(1, 0|\theta)$ into the first result of Eq. (9), we further obtain the optimal working point for phase sensing $\theta_{\min} = 1.7371 \sim \pi/2$ and the best sensitivity $\sqrt{N}\delta\theta_{\min} = 1/\sqrt{F(\theta_{\min})} = 1.0116 \sim 1$, as predicted by Eq. (9). Our results coincide quite well with the experimental data of Ref. [1], where the signal $P(0, 1|\theta) = \sin^2(\theta/2)$ was measured.

TABLE I: For the input states $|1, 0\rangle$ and the twin-Fock states $|n, n\rangle$ with $N = 2n = 2, 4$, and 6 , the parameters used in the simulations are listed as the following.

N	1	2	4	6
(V, h)	(0.994, 0.99)	(0.983, 0.985)	(0.97, 0.98)	(0.94 [4], 0.975)

To simulate the twin-Fock experiments [3, 4], we first write down exact results of the signal for the input states $|1, 1\rangle$, $|2, 2\rangle$, and $|3, 3\rangle$, given by $P(1, 1|\theta) = \cos^2(\theta)$, $P(2, 2|\theta) = [1 + 3\cos(2\theta)]^2/16$ [3], and $P(3, 3|\theta) = [3\cos(\theta) + 5\cos(3\theta)]^2/64$ [4], respectively. Next, we use the parameters shown in Table I to generate N random outcomes. The output signal and the associated phase sensitivity are shown in Fig. 1(c) and (d).

Note that the former two steps in the above simulations, i.e., Eq. (10) and the choice of random outcomes are unnecessary as long as the experimental data has been recorded at hands. One can also note that the sensitivity diverges at certain values of θ . Formally, this is because the slope of signal $\partial P(+|\theta)/\partial\theta = 0$, but the variance of signal $(\Delta\mu)^2 \propto P(+|\theta)[1 - P(+|\theta)] \neq 0$. Here, the outcome “+” represents $n_1 = 1$ and $n_2 = 0$ for the input state $|1, 0\rangle$; While for the twin-Fock states $|n, n\rangle$, it stands for the event $n_1 = n_2 = n$. Due to the experimental imperfections, the signal $P_{\text{fit}}(+|\theta) \neq 0, 1$ at certain values of phase shift (e.g., $\theta = 0, \pm\theta_{\text{dark}}$), so the variance of signal is nonvanishing at that points but the slope of signal is still vanishing, which leads to the singularity of the sensitivity.

Finally, it should be mentioned that, using the method of Ref. [1], the microscopy images can be obtained with the fitting result of $P(+|\theta)$, as depicted in Fig. 2. With a suitable choice of the offset phase φ , the estimator is given by $\phi_{\text{est}}(x, y) = \theta_{\text{est}}(x, y) - \varphi$ [1], where θ_{est} is determined by $P_{\text{fit}}(+|\theta_{\text{est}}) = N_+/N$ at each spatial point.

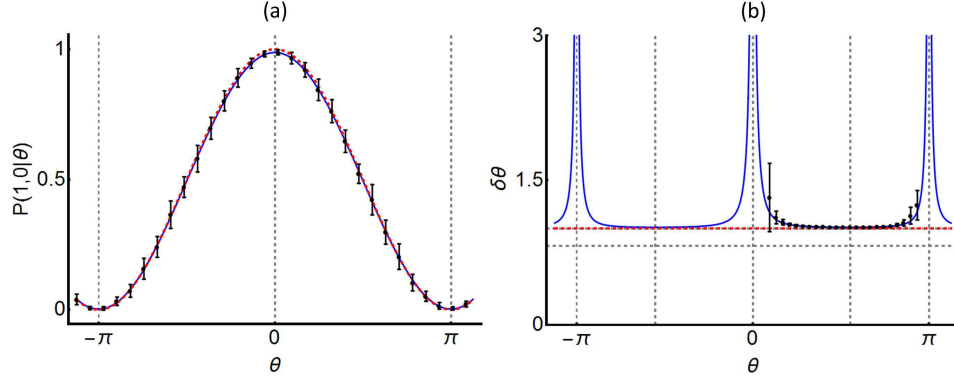


FIG. 5: The conditional probability $P(n_1, n_2|\theta)$ for the input states $|1, 0\rangle$ (a) and the associated phase sensitivity (b). The circles and the bars: statistical averages of $N_{n_1, n_2}/N$ (top) and $\sqrt{N}\sigma_{\text{mle}}$ (bottom), for number of photon counts $N = 100$, and their standard deviations after 20 replicas of the measurements, the same with Fig. 1 in main text. Red dashed and blue solid lines: $P(n_1, n_2|\theta)$ and $P_{\text{fit}}(n_1, n_2|\theta)$, and the associated sensitivities. Vertical lines: locations of the phase origin, the first dark fringe at $\pm\theta_{\text{dark}}$, and the optimal working point for phase sensing at $\pm\theta_{\text{min}}$. The horizontal lines in (b): the shot-noise limit $1/\sqrt{N}$ and $\sqrt{2}/\sqrt{N(N+2)}$ for $N = 1$.

* Electronic address: grjin@bjtu.edu.cn

† Electronic address: wenyang@csrc.ac.cn

‡ Electronic address: cpsun@csrc.ac.cn

[1] Y. Israel, S. Rosen, and Y. Silberberg, Phys. Rev. Lett. **112**, 103604 (2014).

[2] L. Pezze, A. Smerzi, G. Khoury, J. F. Hodelin, and D. Bouwmeester, Phys. Rev. Lett. **99**, 223602 (2007); L. Pezze and A. Smerzi, *ibid.* **100**, 073601 (2008).

[3] F. W. Sun, B. H. Liu, Y. X. Gong, Y. F. Huang, Z. Y. Ou, and G. C. Guo, Europhys. Lett. **82**, 24001 (2008).

[4] G. Y. Xiang, H. F. Hofmann, and G. J. Pryde, Sci. Rep. **3**, 2684 (2013).